Journal of the Korean Electrochemical Society
Vol. 4, No. 1, 2001, 26-33

총 설

Application of Fractal Geometry to Interfacial Electrochemistry - II. Impedance Behaviour of Fractal Electrodes

Heon-Cheol Shin and Su-Il Pyun†

Corrosion and Interfacial Electrochemistry Research Laboratory at Department of Materials Science and Engineering, Korea Advanced Institute of Science and Technology, 373-1 Kusong-Dong, Yusong-Gu, Taejon 305-701, KOREA
(Received February 1, 2001 : Accepted February 21, 2001)

Abstract : This article involves the application of the fractal geometry to interfacial electrochemistry. Especially, we gave our attention to impedance behaviour of the fractal electrode. First, this article briefly explained the constant phase element (CPE) in electrochemical impedance and the de Levie's transmission line model. Second, we introduced the Nyikos and Pajkossy's theoretical works to approach the CPE phenomena using the fractal geometry. Finally this article presented other various fractal models for analysing the ac response of the rough electrodes.

초 록 : 프랙탈 기하학의 계면 전기화학에로의 응용과 관련하여 프랙탈 전극의 임피던스 거동에 대하여 다루었다. 우선, 전기화학적 임피던스 측정시에 자주 관찰되는 constant phase element (CPE)를 간략히 설명하였고, 이와 관련하여 de Levie가 제안한 transmission line model에 대하여 다루었다. CPE현상의 해석을 위하여 Nyikos 와 Pajkossy가 제안한 프랙탈 기하학을 이용한 접근 방법을 소개하였고, 또한 프랙탈 차원과 CPE exponent 사이의 관계를 이론적으로 유도하였다. 마지막으로 rough 혹은 porous 전극의 임피던스 거동을 설명하기 위해 제안된 여러가지 프랙탈 모델들에 대하여 설명하였다.

Key words : Fractal, Rough electrode, Electrochemical impedance spectroscopy, Constant phase element

1. Introduction

Electrochemists have long been puzzled by the appearance of the constant phase element (CPE) or capacitance dispersion in electrochemical impedance of ideally polarisable (*i.e.* blocking) electrode, and considerable effort has been made to understand the origin of the CPE. One of the most possible causes of the CPE is known to be of geometric origin : An irregular and porous electrode geometry causes current density inhomogeneities and thus yields deviations from ideal behaviour.

Most of the contributions to the impedance of the porous electrodes deal with transmission line models.[1-3] The transmission line models usually consider the one-dimensional ionic movement in the electrolyte. Although in some cases[4-7] transmission line models have been more or less successful in explaining the observed impedance behaviour of the porous electrode, the most serious objection to the transmission line model is the implicit assumption that the curvature of the equi-potential surfaces can be neglected in the calculation. That is, the transmission line model can be safely used only for the pores with a depth much larger than their width.

More realistic morphologies can be taken into account by the exact frequency-dependent potential distribution within the entire electrolyte. However, In general these real situations turn out to be much complicated and a straightforward analytical calculation of the overall impedance is usually not possible. In connection with this topic, the fractal geometry has given a powerful tool for the analysis of the CPE behaviour of the rough electrode. A number of theoretical papers[8-21] have devoted to investigate the relationship between the fractal geometry of the electrode and the CPE impedance.

This article explained the transmission line model for the analysis of the CPE impedance. In addition, we introduced the Nyikos and Pajkossy's works on the ac response of the fractal blocking electrode. Finally, this article presented various fractal models for the analysis of the ac response of the rough and irregular electrode.

2. Constant Phase Element (CPE) in Electrochemical Impedance

It has been known for a long time that in the absence of faradaic reactions, the impedance of an electrode in contact with an electrolytic solution usually deviates from the purely capacitive behaviour, and thus simple RC circuit does not give an adequate description of the ac response of the electrode. The electrochemical impedance of a real electrode is frequently represented by an equivalent circuit containing constant phase element (CPE) showing power law frequency dependence as follows :

$$Z(\omega) = (1/\sigma)(j\omega)^{-\alpha} \quad (1)$$

†E-mail: sipyun@mail.kaist.ac.kr

, where σ and α mean the CPE coefficient and the CPE exponent, respectively, and ω represents the angular frequency.

In recent years it has been demonstrated by many researchers that the deviation from ideal capacitive behaviour observed on a real electrode, *i.e.* CPE exponent α is intimately related to surface roughness. Now we focus our attention on those cases when the origin of the CPE behaviour is purely geometrical. Such behaviour has often been found in the porous, rough, and irregular electrode.

The attempt to model the effect of surface roughness on the electrochemical impedance was successfully carried out by de Levie.[1-3] He represented a surface pore by a transmission line as shown in Fig. 1, and derived the following expression for the impedance of the pore, Z_o

$$Z_0 = (1-j)\left(\frac{r}{2\omega c}\right)^{0.5} \coth\left[(1+j)L\left(\frac{\omega rc}{2}\right)^{0.5}\right] \quad (2)$$

, where r and c are resistance and capacitance per unit pore depth, respectively, and L is pore depth. The resultant impedance locus is plotted in Fig. 2. At high frequencies, Eq. (2) reduces to

$$Z_0(high\ freq.) = (1-j)\left(\frac{r}{2\omega c}\right)^{0.5} \quad (3)$$

and the interfacial impedance has a phase angle 45°, whereas at low frequencies Eq. (2) can be written as

$$Z_0(low\ freq.) = \frac{1}{j\omega cL} + \frac{rL}{3} \quad (4)$$

and the phase angle tends towards 90°.

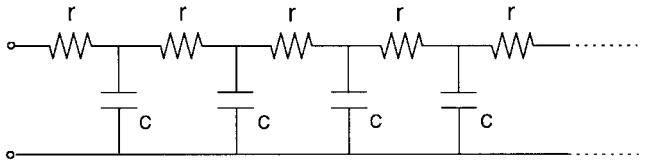

Fig. 1. The equivalent circuit of a pore invaded by a conducting electrolyte (de Levie's transmission line model).

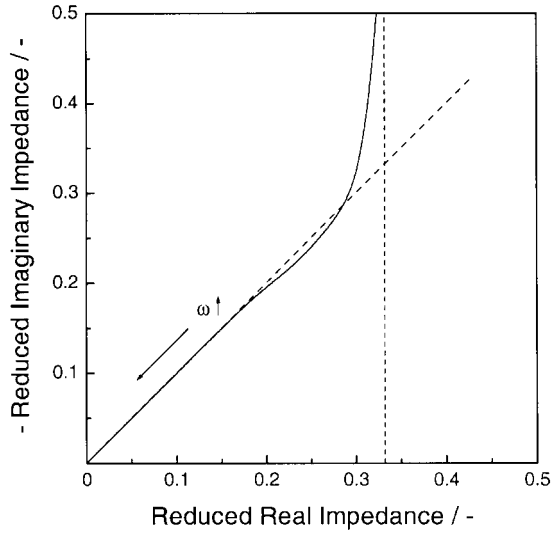

Fig. 2. The complex-plane impedance plot of a cylindrical pore.

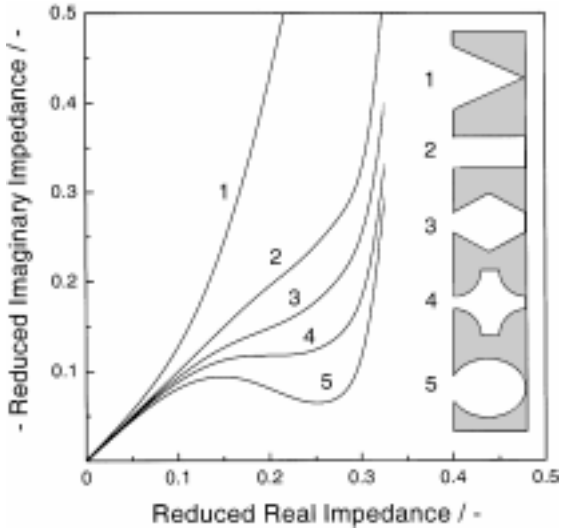

Fig. 3. Pore shapes treated by Keiser *et al.*[4] and corresponding complex-plane impedance plots.

Although de Levie's work succeeds in explaining qualitatively the observed impedance behaviour of the porous electrode, many assumptions and approximations limited the ability of the model to represent accurately the measured impedance data. The assumptions include the cylindrical shape of the pore, the lack of tortuosity of the pore, the lack of distribution of pore sizes and depths, and finally the lack of cross linking between pores.

Over the years, many attempts have been made to improve de Levie's cylindrical pore model. Especially Keiser *et al.*[4] showed that the more occluded the shape of the pore, the more the impedance locus was distorted from capacitive behaviour (Fig. 3). Nevertheless, although the total impedance will reflect more or less the shape of the individual pore, the single pore models still do not account for the effects of the random distribution of pores on the surface and the random variations in pore geometry or the complicated surface topology. Many researchers tried to modify the single pore model on various assumptions about pore distribution and pore size, *etc.*[22,23] However, the increased complexity of the models and many assumptions would tend to undermine its credibility and usefulness, and to prevent one from drawing meaningful conclusions.

3. Ac Response of Fractal Blocking Electrodes : Nyikos and Pajkossy's Works

The situation changed drastically in the mid-1980s after Mandelbrot's book[24] on fractals. The first papers based upon the fractal geometry appeared claiming that solid surfaces (both porous and rough) can be modelled by fractals.[25-27] Since those works, the questions raised by many theoreticians were whether or not the impedance response of capacitive electrodes of the fractal geometry is of CPE type, and if it is, whether or not there is some correlation between the CPE exponent α and the fractal dimension D_H.

Many fractal models have been developed to give the

answer. One group of fractal models is based upon the scaling laws of surface capacitance and solution resistance. Since dilatational symmetry is a basic feature of fractals, one can set up equations which relate the system size and the frequency dependence of impedance. Another group of fractal models has been developed by generalising the pore models by assuming branching pores or by introducing a fractal size distribution of an ensemble of pores or caves. These models have become fairly popular because the impedance can be calculated easily. In this Section, we explain the former group of the models (especially the model by Nyikos and Pajkossy[11]), and in the following Section, we present the latter group of the models.

Nyikos and Pajkossy[11] started by noting that any two-terminal RC network can be written as the parallel combination of a number of series RC circuits. For one such series circuit, the elementary admittance is expressed as

$$Y_k = (Z_k)^{-1} = \left(R_k + \frac{1}{j\omega C_k}\right)^{-1} = \frac{j\omega C_k}{1 + j\omega R_k C_k} \tag{5}$$

so that the admittance of the entire parallel assembly follows as

$$Y = \sum_k Y_k = \sum_k \frac{j\omega C_k}{1 + j\omega R_k C_k} \tag{6}.$$

The R_k and C_k are elementary resistance and capacitance, respectively. Now let us enlarge the whole system in each spatial direction by a factor of m. Since Y is a macroscopic quantity and the electrode is macroscopically two-dimensional, Y scales in the following way

$$Y(m, \omega) = m^2 Y(1, \omega) \tag{7}$$

, where the first argument denotes system size. Next, since capacitance is proportional to area and the area changes as m^{D_H}, the scaling law for the microscopic C_k element takes the form

$$C_k(m) = m^{D_H} C_k(1) \tag{8}.$$

Finally the element R_k scales in the usual way

$$R_k(m) = m^{-1} R_k(1) \tag{9}.$$

From the combination of Eqs. (6), (8) and (9), we have

$$\begin{aligned} Y(m, \omega) &= \sum_k \frac{j\omega C_k(m)}{1 + j\omega R_k(m) C_k(m)} \\ &= m \sum_k \frac{j(\omega m^{D_H - 1}) C_k(1)}{1 + j(\omega m^{D_H - 1}) R_k(1) C_k(1)} \\ &= m Y(1, \omega m^{D_H - 1}) \end{aligned} \tag{10}.$$

Substituting Eq. (10) into Eq. (7), we get

$$\frac{Y(1, \omega m^{D_H - 1})}{Y(1, \omega)} = m \tag{11}.$$

Alternatively we obtained easily the following equation from Eq. (1).

$$\begin{aligned} \frac{Y(1, \omega m^{D_H - 1})}{Y(1, \omega)} &= \frac{1/Z(1, \omega m^{D_H - 1})}{1/Z(1, \omega)} \\ &= \frac{\sigma(j\omega m^{D_H - 1})^{\alpha}}{\sigma(j\omega)^{\alpha}} = (m^{D_H - 1})^{\alpha} \end{aligned} \tag{12}$$

Then, from Eqs. (11) and (12), we finally obtain

$$\alpha = \frac{1}{D_H - 1} \tag{13}.$$

Thus, the CPE exponent α becomes the measure of surface irregularity. For example, for a perfectly smooth surface with $D_H = 2$ at all scales, Eq. (13) predicts $\alpha = 1$, *i.e.* purely capacitive behaviour. In other limit as $D_H \rightarrow 3$, $\alpha \rightarrow 0.5$ which is de Levie's well-known result for the electrode with cylindrical pore. Eq. (13) also implies that surfaces with different morphologies but with the same fractal dimension are equivalent as far as impedance is concerned.

4. Various Fractal Models for Ac Response of Rough Blocking Electrodes

4.1. Sierpinski fractal electrode I : *Nyikos and Pajkossy's model*[21]

The cell geometry is based on the Sierpinski carpet or gasket (Fig. 4 (a)-(c))[24] characterised by the ratio N of the number of pores generated at stage n to that number at stage n-1, and the reduction ratio m of the side lengths of pores at consecutive stages. The fractal dimension of the carpet or gasket, D_S, is given as $D_s = \ln(N)/\ln(m)$. The Sierpinski electrode is con-

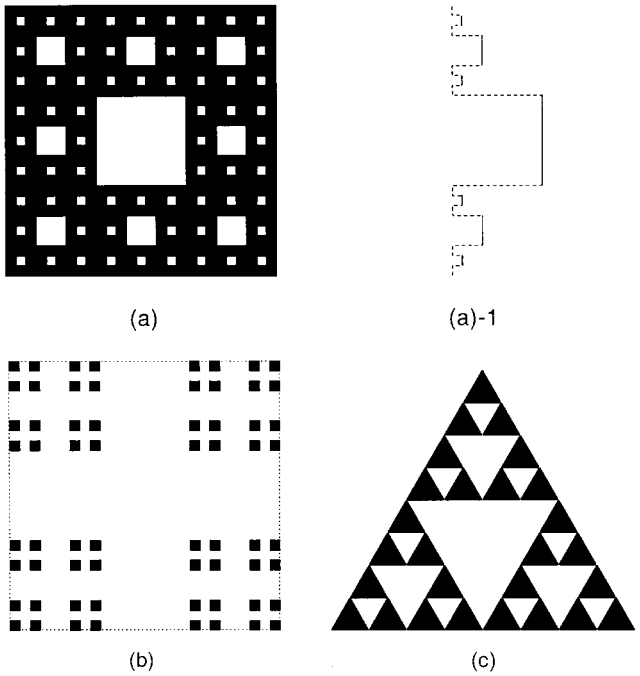

Fig. 4. Various Sierpinski electrodes with the fractal dimension D_S of (a) 1.8928, (b) 1.2619, and (c) 1.5850. (a)-1 represents the horizontal cross section of electrode (a).

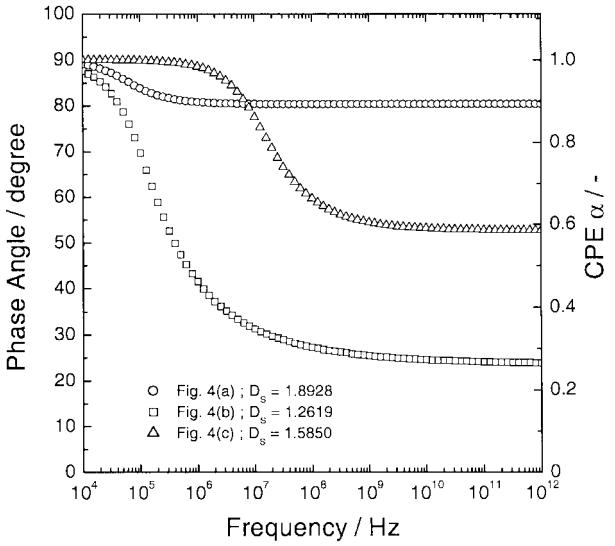

Fig. 5. The variation of phase angle with frequency at three different Sierpinski electrodes of Fig. 4. It was assumed that the side length of the electrode is 1 cm, the resistivity of the electrolyte is 0.05 Ωcm, and the double layer capacitance per unit area of the electrode/ electrolyte interface is 10^{-4} Fcm^{-2}.

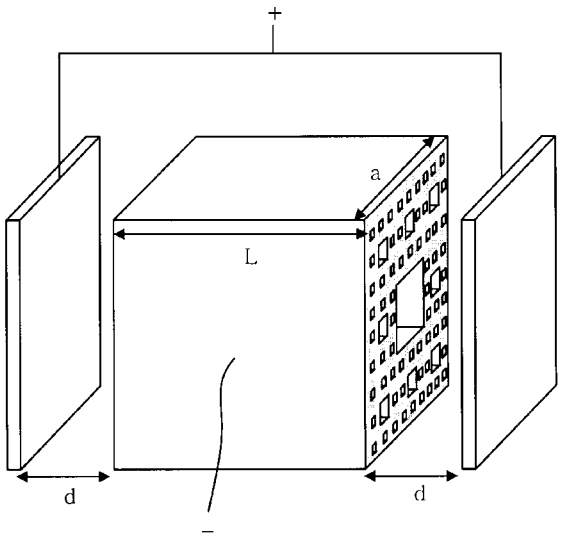

Fig. 6. The configuration of the Sierpinski working electrode and counter electrodes.

structed by fitting each pore of cubic shape in its horizontal cross section, as depicted in Fig. 4(a)-1. The bottom interface of each pore is assumed to be capacitive (solid line in Fig. 4(a)-1) and the other sides insulating (dotted line in Fig. 4(a)-1). The counter electrode is assumed to be located just in front of the Sierpinski electrode, which means that the individual pores are independent, and their equivalent circuit is a series RC circuit.

Let the solution resistance and the double layer capacitance of the largest pore be denoted by R_0 and C_0, respectively. Then, the capacitance and resistance of the kth-order (or k-staged) pore equal C_0/m^{2k} and R_0m^k, respectively, and the number of kth-order pores is N^k. Thus, the total admittance of the cell is given by

$$Y(\omega) = \sum_{k=0}^{\infty} \frac{1}{R_0 m^k N^{-k} + (j\omega C_0 m^{-2k} N^k)^{-1}} = \sum_{k=0}^{\infty} \frac{j\omega C_0 m^{-2k} N^k}{j\omega C_0 R_0 m^{-k} + 1} \quad (14).$$

When the frequency ω goes towards infinity, the admittance becomes $Y = c_1(j\omega C_0 R_0)^{\alpha}$, where $c_1 = \pi/[R_0 \ln(m) \sin(\alpha\pi)]$ and $\alpha = \ln(N/m)/\ln(m) = D_s\text{-}1$. Thus this type of the Sierpinski electrode shows CPE behaviour with the exponent $\alpha = D_s\text{-}1$. The variation of phase angle with frequency is plotted at 3 different Sierpinski electrodes (Fig. 4(a)-(c)) in Fig. 5.

4.2. Sierpinski fractal electrode II : *Chu's model*[14-16]

Let us consider the cell configuration of Fig. 6. The working electrode is the Sierpinski carpet of the fractal dimension $D_s = \ln N/\ln m$ in its cross section. Only the walls of the pores are assumed to be capacitive. If the solution resistance between working and counter electrodes is taken into account, the elementary impedance Z_k for a single pore is given by

$$Z_k = \frac{2d\rho}{a_k^2} + \left(\frac{\rho\lambda_k}{2a_k^2}\right) \coth\left(\frac{L}{2\lambda_k}\right) \quad (15)$$

with $\lambda_k^{-1} = (2\xi\rho\omega/a_k)^{1/2}(1+j)$, and $a_k = a/m^k$, where ρ is the resistivity of the electrolyte; ξ, the capacitance per unit area of the electrode surface; a_k, the side length of the pore at the kth-order; d, the distance between working and counter electrodes, and L represents the length of the Sierpinski electrode. The first term of Eq. (15) is the resistance due to the solution outside the pore, and the second term is the impedance due to the single pore in the working electrode.[14)]

Now, the second term of Eq. (15) can be written as $(\rho\lambda_k/2a_k^2)\coth(L/2\lambda_k) \approx \rho L/12a_k^2 + (4j\omega a_k L\xi)^{-1}$ at sufficiently low frequencies. It is noted that the first term in the above equation represents a resistor with resistance $\rho L/12a_k^2$ and the second term represents a capacitor with capacitance $4a_kL\xi$. Substituting the above equation into Eq. (15), we get

$$Z_k \approx \frac{\rho}{a_k^2}\left(2d + \frac{L}{12}\right) + (4j\omega a_k L\xi)^{-1} \quad (16).$$

That is, in the low frequency limit the elementary impedance of the combination of a single pore and the solution outside the pore can be represented by a capacitor in series with a resistor.

Then, the total impedance is given by

$$Z_n(\omega) = (Y_n)^{-1} = \left(\sum_{k=1}^{n} \frac{N^{k-1}}{Z_k}\right)^{-1} = \frac{r_1(N/m-1)^2}{N-1}\frac{N^n}{(N/m)^{2n}} + \frac{N/m-1}{j\omega c_1 (N/m)^n} \quad (17)$$

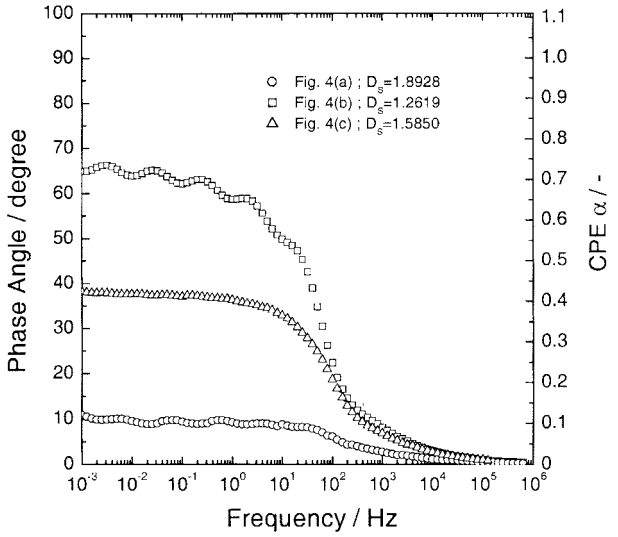

Fig. 7. The variation of phase angle with frequency at three different Sierpinski electrodes. It was assumed that a = 0.1 cm, d = 0.1 cm, and L = 1 cm.

, where r_1 and c_1 are defined as $\rho(2d + L/12)/a_1^2$ and $4\xi La_1$, respectively, and the subscript n indicates the total number of stages. From Eq. (17) we easily obtain the following relation

$$Z_n\left(\frac{\omega}{m}\right) = \left(\frac{m^2}{N}\right)Z_{n-1}(\omega) \qquad (18).$$

For extremely large n, the small-ω expansion eventually breaks down, but the relation in Eq. (18) remains valid[10] and approaches the dynamic scaling law

$$Z\left(\frac{\omega}{m}\right) = \left(\frac{m^2}{N}\right)Z(\omega) \qquad (19)$$

, where $Z(\omega) = \lim_{n\to\infty} Z_n$. Since the solution of Eq. (19) is $Z(\omega) \propto \omega^{\alpha}$ at sufficiently low frequencies, we obtain

$$\alpha = 2 - \frac{ln(N)}{ln(m)} = 2 - D_S \qquad (20).$$

Fig. 7 shows the variation of phase angle with frequency at 3 different Sierpinski electrodes with the cross sections of Fig. 4(a)-(c), calculated on the basis of Eq. (15). The phase angles at the low frequencies are equal to be those predicted by Eq. (20).

4.3. Cantor fractal electrode I : *Liu's model*[10]

The cross section of the electrode used in this model is depicted in Fig. 8. The electrolyte and the electrode are shown in black and white, respectively. The grooves in the electrode are seen as protrusions on the electrolyte side. Each groove has the self-similar structure in that it subdivides into two branches, and the branches are similar to the whole groove when magnified by a factor m. Viewed from the electrolyte side, the interface is regarded as the Cantor bar[24], whose fractal dimension is $D_c = \ln 2/\ln m$. The model can be generalised to N grooves, each of which subdivides into N branches at every stage. The scale factor m satisfies $m > N$ and thus $D_c = \ln N/\ln m < 1$. It is assumed that only the walls of the grooves are capacitive.

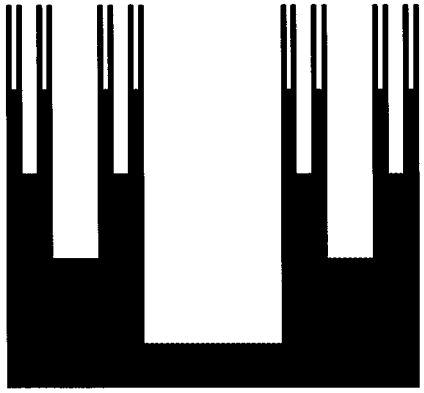

Fig. 8. Cantor fractal model of a rough interface between an electrolyte (black) and an electrode (white).

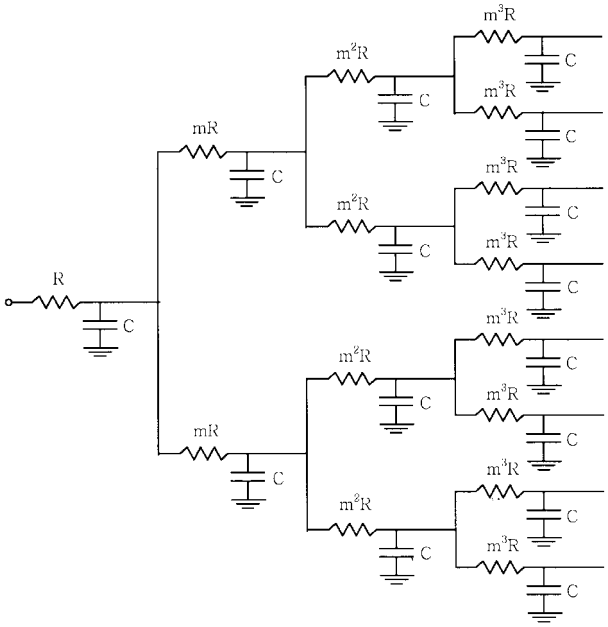

Fig. 9. Equivalent circuit for the Cantor fractal model of Fig. 8.

The electrical properties of this structure can be analysed by constructing an electric circuit analogue of Fig. 9. Since the cross section area of the grooves is reduced by the ratio $1/m$ at every stage of branching, whereas the depth of the grooves is invariant, the resistance R increases by the ratio m at every stage. The common ground is the electrode.

The impedance of the electric circuit of Fig. 9 has the form of an infinite continued fraction:

$$Z(\omega) = R + \cfrac{1}{j\omega C + \cfrac{2}{mR + \cfrac{1}{j\omega C + \cfrac{2}{m^2R + \cfrac{1}{j\omega C + \cdots}}}}} \qquad (21)$$

It can be readily verified for $\omega RC \ll 1$ that $Z_1(\omega) = R + 1/$

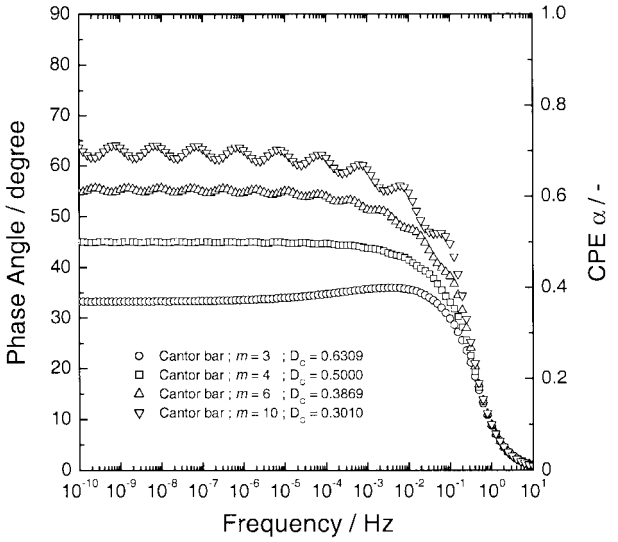

Fig. 10. The variation of phase angle with frequency at four different Cantor electrodes. It was assumed that the side length of the electrode is 1 cm.

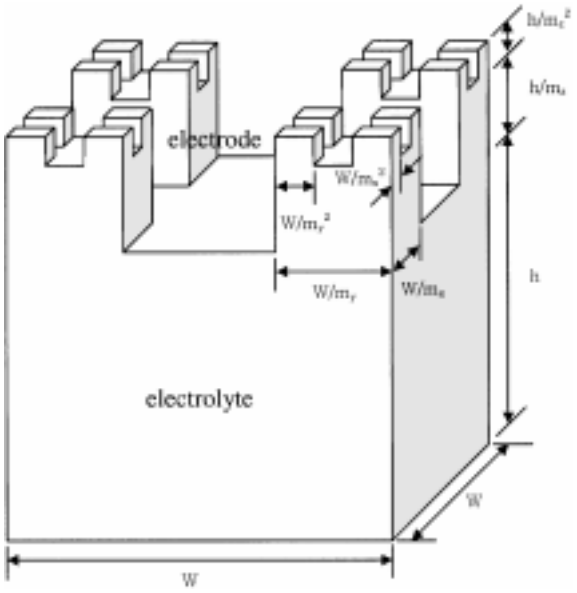

Fig. 11. Self-affine Cantor fractal model of a rough interface between an electrolyte and an electrode.

$j\omega C$, $Z_2(\omega) \cong R(1 + 2m/9) + 1/3j\omega C$, …, where the subscript means the number of branching step. After a sufficiently large number of branching steps, $n \gg 1$, and for $m > 2$, $\omega RC \ll 1$, the impedance can be written approximately as

$$Z_n \cong R\frac{m(m+1)}{(m-1)(m-2)(2m-1)}\left(\frac{m}{2}\right)^n + \frac{1}{2^n j\omega C} \quad (22).$$

From Eq. (22) it is seen that

$$Z_n\left(\frac{\omega}{m}\right) = \frac{m}{2}Z_{n-1}(\omega) \quad (23).$$

For large n, Eq. (18) approaches the dynamic scaling law

$$Z\left(\frac{\omega}{m}\right) = \frac{m}{2}Z(\omega) \quad (24)$$

, where $Z(\omega) = \lim_{n\to\infty} Z_n$. Since the solution of Eq. (24) is $Z(\omega) \propto \omega^{-\alpha}$ at sufficiently low frequencies, we obtain

$$\alpha = 1 - \frac{ln(2)}{ln(m)} = 1 - D_C \quad (25).$$

Fig. 10 shows the variation of phase angle with frequency at various m values, calculated on the basis of Eq. (21). The phase angles at the low frequencies are equal to be those predicted by Eq. (25).

4.4. Cantor fractal electrode II : *generalised Liu's model*[13,19]

Finally, we examine the self-affine[24,28] fractal model. The cell configuration is shown in Fig. 11, which generalises the model of Section 4.3. The electrolyte protrudes into the electrode. At each successive stage, N_xN_y new branches appear which are scaled in depth and width by $1/m_x$ and $1/m_y$, respectively, and in height by $1/m_z$. N_x is the number of new branches appearing at each stage of the structure created by projecting the Cantor block on the x-z plane, and N_y, on the y-z plane. m_x, m_y and m_z mean the reduction ratios in the direction of x, y, and z, respectively. By geometry, $m_x > N_x$ and $m_y > N_y$. It is assumed that only the walls of the branches are capacitive.

The electric circuit analogue of this cell is constructed as tree structure with N_xN_y new branches appearing at each new node. Each branch has a series resistor and a capacitor connected to ground. The resistance R increases by m_xm_y/m_z in each successive stage, due to the reduction in cross-sectional area of the branch by $1/m_xm_y$ and the decrease in length by $1/m_z$. Similarly, the capacitance C is reduced by $(1/m_x+1/m_y)1/m_z$ since the interfacial areas of the walls on the x-z and y-z planes are reduced by $1/m_xm_z$ and $1/m_ym_z$, respectively, in successive stages. The electric circuit of the interface is shown in Fig. 12, which circuit describes the special case of $m_x = m_y = m$, $m_z = 1$, and $N_x = N_y = 2$.

The input impedance of this circuit has the form of a following infinite continued fraction

$$Z(\omega) = R + \cfrac{1}{j\omega C + \cfrac{N_xN_y}{\cfrac{m_xm_y}{m_z}R + \cfrac{1}{j\omega\frac{C}{m_z}\left(\frac{1}{m_x}+\frac{1}{m_y}\right) + \cfrac{N_xN_y}{\left(\frac{m_xm_y}{m_z}\right)^2 R + \cfrac{1}{j\omega\frac{C}{m_z^2}\left(\frac{1}{m_x^2}+\frac{1}{m_y^2}\right) + \cdots}}}}} \quad (26).$$

The model can be solved for three different cases. In the first case, we let $m_x = m_y = m$, $m_z = 1$, and $N_x = N_y = N$. From Eq. (26), then we find

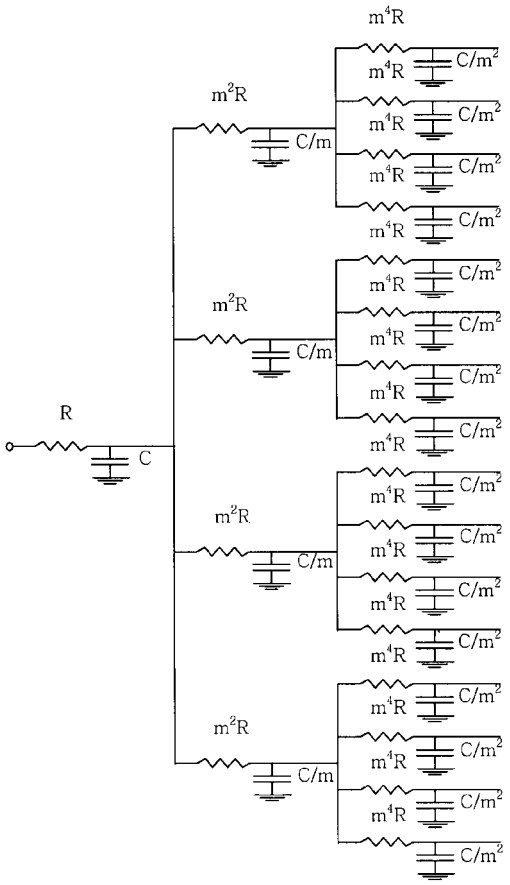

Fig. 12. Equivalent circuit for the self-affine Cantor fractal model of Fig. 11. It was assumed that $m_x = m_y = m$, $m_z = 1$ and $N_x = N_y = 2$.

$$Z\left(\frac{\omega}{m}\right) = R + \frac{m^2 Z(\omega)}{j\omega m C Z(\omega) + N^2} \quad (27).$$

Under the assumption that $Z(\omega) \rightarrow \infty$ and $\omega Z(\omega) \rightarrow 0$ as $\omega \rightarrow 0$, Eq. (27) becomes

$$Z\left(\frac{\omega}{m}\right) = \frac{m^2}{N^2} Z(\omega) \quad (28).$$

Since the solution of Eq. (28) is $Z(\omega) \propto \omega^{\alpha}$ and the fractal dimension D of the surface is determined, by measuring the total surface area at different scales,[13] to be $D = \ln(N^2)/\ln m + 1$, we obtain

$$\alpha = 2 - \frac{ln(N^2)}{ln(m)} = 3 - D \quad (29).$$

In the next case, we let $m_x > m_y$ and $m_z = 1$. For this case, Eq. (26) says that the capacitive term is dominated by the $(1/m_y)^n$ term. Keeping in mind that it is not the few beginning terms that determine α, but the infinite tail of the continued fraction, we can concentrate only on that part of the continued fraction where the m_y term dominates. Solving Eq. (26) as in the first case and then taking the fractal dimension of the surface as $D = 2 + \ln(N_x N_y/m_y)/\ln(m_x)$, we find

$$\alpha = 1 - \frac{ln(N_x N_y/m_y)}{ln(m_x)} = 3 - D \quad (30).$$

Finally, consider the most general case: $m_x > m_z$ and $m_x > m_y$. Treating the impedance Eq. (26) as in the first case, we find

$$\alpha = 1 - \frac{ln(N_x N_y/m_y m_z)}{ln(m_x/m_z^2)} \quad (31).$$

In this case, the fractal dimension of the surface is calculated to be $D = 2 + \ln(N_x N_y/m_y m_z)/\ln(m_x)$. Then, α is not related to the fractal dimension D.

5. Concluding Remarks

The present article explained first the constant phase element (CPE) in electrochemical impedance and second briefly introduced the Nyikos and Pajkossy's work[11] on the charging /discharging of the fractal blocking electrode. Finally, this article summarised various fractal models for analysing the ac response of the rough electrodes. On the basis of the fractal geometry, one can quantitatively estimate the fractal dimension of the electrode surface using the electrochemical impedance spectroscopy.

As a matter of fact, it is still a troublesome issue to relate the determined fractal dimension with the surface roughness of the electrode: Even on single crystalline surface, defects of the crystal structure may cause local capacitive inhomogeneities, thus causing non-ideal capacitive behaviour. This is especially true when real rough surfaces with lots of crystal defects and dislocations, *etc*. are considered. These surface inhomogeneities cause additionally the time constant distributions, and thus lower the phase angle of the impedance. Under these complicated circumstances, the time constant distributions may give more meaningful information than the fractal dimension does, about the origin of the abnormal electrochemical response of the electrode to ac signal.[29-31]

References

1. R. de Levie, *Electrochim. Acta*, **9**, 1231 (1964).
2. R. de Levie, *Electrochim. Acta*, **10**, 113 (1965).
3. R. de Levie, in Advances in Electrochemistry and Electrochemical Engineering, Edited by P.Delahay, Vol. VI, 329, John Wiley, New York (1967).
4. H. Keiser, K. D. Beccu and M. A. Gutjahr, *Electrochim. Acta*, **21**, 539 (1976).
5. J. -P. Candy, P. Fouillox, M. Keddam and H. Takenouti, *Electrochim. Acta*, **26**, 1029 (1981).
6. T. Ohmori, T. Kimura and H. Masuda, *J. Electrochem. Soc.*, **144**, 1286 (1997).
7. K. Honda, T. N. Rao, D. A. Tryk, A. Fujishima, M. Watanabe, K. Yasui and H. Masuda, *J. Electrochem. Soc.*, **147**, 659 (2000).
8. A. Le Mehaute and G. Crepy, *Solid State Ionics*, **9&10**, 17 (1983).
9. A. Le Mehaute, *J. Stat. Phys.*, **36**, 665 (1984).
10. S. H. Liu, *Phys. Rev. Lett.*, **55**, 529 (1985).

11. L. Nyikos and T. Pajkossy, *Electrochim. Acta*, **30**, 1533 (1985).
12. T. C. Halsey, *Phys. Rev. A*, **35**, 3512 (1987).
13. T. Kaplan, L. J. Gray and S. H. Liu, *Phys. Rev. B*, **35**, 5379 (1987).
14. B. Sapoval, *Solid State Ionics*, **23**, 253 (1987).
15. Y. T. Chu, *Solid State Ionics*, **26**, 299 (1988).
16. R. M. Hill and L. A. Dissado, *Solid State Ionics*, **26**, 295 (1988).
17. W. H. Mulder and J. H. Sluyters, *Electrochim. Acta*, **33**, 303 (1988).
18. J. C. Wang, *Electrochim. Acta*, **33**, 707 (1988).
19. M. Blunt, *J. Phys. A: Math. Gen.*, **22**, 1179 (1989).
20. A. Maritan and F. Toigo, *Electrochim. Acta*, **35**, 141 (1990).
21. T. Pajkossy and L. Nyikos, *Phys. Rev. B*, **42**, 709 (1990).
22. W. Scheider, *J. Phys. Chem.*, **79**, 127 (1975).
23. M. Kramer and M. Tomkiewicz, *J. Electrochem. Soc.*, **131**, 1283 (1984).
24. B. B. Mandelbrot, "The Fractal Geometry of Nature", 1, 80, 131, Freeman, New York (1983).
25. D. Avnir, D. Farin and P. Pfeifer, *J. Chem. Phys.*, **79**, 3566 (1983).
26. P. Pfeifer and D. Avnir, *J. Chem. Phys.*, **79**, 3558 (1983).
27. D. Avnir, D. Farin and P. Pfeifer, *Nature*, **308**, 261 (1984).
28. A. -L. Barabasi and H. E. Stanley, "Fractal Concepts in Surface Growth", 32, Cambridge University Press, New York (1995).
29. J. R. Miller, in Proceedings of the Symposium on Electrochemical Capacitors, Edited by F.M.Delnick and M.Tomkiewicz, PV 95-29, The Electrochemical Society Proceeding Series, 246, Pennington, NJ (1995).
30. D. Qu and H. Shi, *J. Power Sources*, **74**, 99 (1998).
31. B. E. Conway, "Electrochemical Supercapacitors: Scientific Fundamentals and Technological Applications", 545, Kluwer Academic/ Plenum Publishers, New York (1999).